



ELSEVIER

15 October 2001

Physics Letters A 289 (2001) 111–120

PHYSICS LETTERS A

www.elsevier.com/locate/pla

Amplitude equations for non-linear Rayleigh waves

Panayotis Panayotaros

Department of Applied Mathematics, UCB 526, University of Colorado at Boulder, Boulder, CO 80309-0526, USA

Received 21 June 2001; received in revised form 30 August 2001; accepted 31 August 2001

Communicated by C.R. Doering

Abstract

We investigate asymptotic equations describing small amplitude surface elastic waves in the half-plane (Rayleigh waves). For hyperelastic materials such model equations are Hamiltonian systems, and are seen to lead to the formation of singularities in the surface elastic displacement. At the time of singularity formation the Fourier spectra of the solutions exhibit power law decay, and the observed exponents suggest the existence of both differentiable and non-differentiable singular profiles. © 2001 Elsevier Science B.V. All rights reserved.

1991 MSC: 74J30; 74J15; 74H10; 74H35

Keywords: Rayleigh waves; Multiple scales; Integral operators; Singularity formation

1. Introduction

In this Letter we study the non-linear evolution of small amplitude periodic surface elastic waves (Rayleigh waves) in the half-plane. Early investigations of non-linear Rayleigh waves in this geometry have focused on the question of existence of traveling waves of permanent form (see [1,2]), reducing the full traveling wave equation to a simpler model. We have recently seen that traveling waves solutions of such model equations can have non-smooth profiles (see [3]) and in this work we extend our investigation of singularities in Rayleigh waves to the evolution problem.

To study the evolution problem we use an asymptotic amplitude equation originally derived in [4] (see also [5]) that describes the non-linear slow modulation of linear Rayleigh waves. In this approximation, the

motion of the solid is described by the evolution of the surface elastic displacement. The resulting amplitude equation is non-local and has the structure of a non-local Hamilton–Jacobi type equation. Equations with a similar structure can be derived for other systems, e.g., for conservation laws in the half-plane and other scale invariant interface geometries (see, e.g., [6]). Also, non-linear Rayleigh waves have been recently generated and studied experimentally (see [7,8]), and we comment on the relation of the present work with these experiments the end of the Letter.

Numerical simulations in [4,9] and elsewhere show that the amplitude equations for surface elastic waves can develop singularities. To investigate these singularities we consider hyperelastic materials, where the amplitude equations have a Hamiltonian structure. We study numerically three hyperelastic models and in all cases we see that smooth initial conditions lead to non-smooth surface elastic displacements. These phenomena are especially pronounced for the horizontal displacement, where we see the formation of “cusps”, i.e.,

E-mail address: panos@colorado.edu (P. Panayotaros).

points where the second derivative of the horizontal elastic displacement diverges. We argue that for analytic initial conditions the solutions stay analytic up to the time of singularity formation. As a consequence, the Fourier spectra of the solutions have power law decay at the singularity formation time, and this observation allows us to determine the singularity time numerically. Note that the idea of connecting singularity formation, loss of analyticity and Fourier spectra has been used by several authors (see, e.g., [10,11]). Since characteristics or similarity blow-up solutions are not available here, we focus on the evolution of Fourier spectra.

Power law exponents at the singularity time can be measured in several ways, in some cases using the conservation of momentum. The exponents observed suggest that for some initial conditions the surface elastic displacement is still differentiable at the singularity time, i.e., the apparent “cusps” are differentiable functions. For other initial conditions, however, the elastic displacement at the singularity time may fail to be differentiable. We also remark that the traveling wave solutions seen in [3] have even stronger singularities.

This Letter is organized as follows. Section 2 sets up the notation and outlines the argument leading to the amplitude equations. In Section 3 we show that the amplitude equations have a Hamiltonian structure, and we discuss some of their symmetries. In Section 4 we describe numerical experiments with three models, focusing at the power law behavior at the time of singularity formation. In the last section we briefly discuss to connection of our work with recent experiments on non-linear Rayleigh waves.

2. Amplitude equation for surface elastic waves

We consider \mathbf{R}^2 with the Cartesian coordinates (x_1, x_2) and an elastic solid occupying in its undeformed state the half-plane $H = \{x = (x_1, x_2) \in \mathbf{R}^2: x_2 \geq 0\}$. The Cartesian components of the elastic displacement u will be denoted by $u_i(x_1, x_2)$, $i = 1, 2$. The density ρ of the material will be assumed to be constant. The internal elastic forces due to a deformation can be obtained from the (first Piola–Kirchhoff) stress tensor $\tau(x) : H \rightarrow \mathbf{R}^2 \times \mathbf{R}^2$, thought of here as a 2×2 real matrix with components τ_{ij} , $i, j = 1, 2$. We will assume that the stress tensor τ is a specified func-

tion $\tau(\nabla u)$ of the derivative ∇u of the elastic displacement ($\tau(\nabla u)$ is the “stress–strain” relation). With this notation, a time-dependent elastic displacement must satisfy the equations of motion

$$\rho \partial_{tt} u_i = \sum_{j=1}^2 \partial_{x_j} \tau_{ij}, \quad i = 1, 2, \quad \text{in } H, \quad (2.1)$$

and we will consider “zero-traction” boundary conditions

$$\sum_{j=1}^2 \tau_{ij} \hat{n}_j = 0 \quad \text{at } \partial H, \quad (2.2)$$

with $\hat{n} = [\hat{n}_1, \hat{n}_2] = [0, -1]$ the outward unit normal at ∂H . A convenient shorthand for (2.1), (2.2) is $\rho \partial_{tt} u = \nabla \cdot \tau$ in H , $\tau \cdot \hat{n} = 0$ at ∂H , respectively.

We will also require that for all times $t \in \mathbf{R}$ the elastic displacement satisfy periodicity and decay conditions

$$u(x_1 + 2\pi, x_2, t) = u(x_1, x_2, t), \quad \forall (x_1, x_2) \in H, \quad (2.3)$$

$$\lim_{x_2 \rightarrow \infty} u(x_1, x_2, t) = 0, \quad \forall x_1 \in \mathbf{R}, \quad (2.4)$$

respectively. In view of the periodicity condition in the horizontal direction we work in the half-cylinder D , obtained by identifying the points $(x_1 + \pi, x_2)$ and $(x_1 - \pi, x_2)$ of the strip $\tilde{D} = \{(x_1, x_2) \in H: x_1 \in [-\pi, \pi]\}$.

We will be particularly interested in hyperelastic materials, where the stress tensor τ has the form

$$\tau_{ij} = \frac{\partial W(\nabla u)}{\partial u_{i,j}}, \quad \text{with } u_{i,j} = \partial_{x_i} u_j, \quad i, j = 1, 2. \quad (2.5)$$

The real function W represents the density of the potential energy stored in a deformed solid. We will assume that the potential energy density can be decomposed as $W = W^L + W^{\text{NL}}$, with W^L quadratic and W^{NL} cubic in ∇u . The quadratic part W^L will be given by

$$W^L = \frac{\lambda}{2} (\text{tr } \gamma)^2 + \mu \text{tr}(\gamma^2), \quad \text{with} \\ \gamma = \frac{1}{2} [\nabla u + (\nabla u)^T], \quad (2.6)$$

with $\lambda, \mu > 0$ the Lamé constants. The particular choice of W^L gives the standard linear theory for iso-

tropic materials. Also, we let

$$W^{\text{NL}} = \sum_{a,b,c,d,e,f=1}^2 W_{abcdef}^{\text{NL}} u_{a,b} u_{c,d} u_{e,f}, \quad (2.7)$$

with the W_{abcdef}^{NL} real constants. The cubic part W^{NL} is general enough to include the cubic part of several physically reasonable models, e.g., for isotropic materials. An example is the St. Venant–Kirchhoff material, considered in Section 4. The asymptotic theory below describes only the lowest-order non-linear effects and does not take into account the effects of quartic or higher-order terms in the potential energy density.

We will now use a formal multiple scales argument to seek small amplitude solutions of (2.1)–(2.3) that have the form

$$u(x_1, x_2, t) = \epsilon U(\theta, x_2, \epsilon t) + \epsilon^2 \tilde{U}(\theta, x_2, \epsilon t) + O(\epsilon^3), \quad (2.8)$$

where $\theta = x_1 - ct$, and c is a constant. We enforce the boundary conditions (2.3), (2.4) by requiring that U, \tilde{U} be 2π -periodic in θ , and that they decay as $x_2 \rightarrow \infty$. The small parameter ϵ can be chosen to be the typical slope $\partial_{x_1} u_1$ of the horizontal displacement. We are thus seeking elastic displacements that travel to the right with velocity c , with a wave profile that varies over a “slow” time-scale ϵt . The goal is an equation describing the slow evolution of $U(\theta, x_2, \epsilon t)$. Equations of this type have been derived by [4]. The argument we outline here follows related work of [6].

To determine U, \tilde{U} we insert (2.8) into Eqs. (2.1), (2.2) and match powers of ϵ . Note that $\partial_\theta = \partial_{x_1}$ and $\partial_t = \partial_{T_0} + \epsilon \partial_T + O(\epsilon^2)$, i.e., $T_0 = t$ and $T = \epsilon t$, are the “fast” and “slow” time-scales, respectively. At order ϵ^1 we have the linear homogeneous system

$$(\lambda + \mu) \nabla (\nabla \cdot U) + \mu \Delta U - \rho c^2 \partial_\theta^2 U = 0 \quad \text{in } D, \quad (2.9)$$

and

$$\begin{aligned} -\mu (\partial_{x_2} U_1 + \partial_\theta U_2) &= 0, \\ -\lambda (\nabla \cdot U) - 2\mu \partial_{x_2} U_2 &= 0 \quad \text{at } \partial D, \end{aligned} \quad (2.10)$$

with $\nabla = [\partial_\theta, \partial_{x_2}]$ and $\Delta = \nabla \cdot \nabla$. We also require that $U(\theta, x_2) \rightarrow 0$ as $x_2 \rightarrow \infty$. Eqs. (2.9), (2.10) do not involve T so that the dependence of solutions on T is arbitrary at this stage.

The theory of (2.9), (2.10) is well known (see, e.g., [12,13]), and we summarize the results. First, in order for solutions with the required boundary conditions to exist, c^2 must satisfy a cubic equation with a unique real solution c_0^2 (the Rayleigh speed). Then, letting

$$A^2 = 1 - \frac{\rho c_0^2}{\mu} \quad \text{and} \quad B^2 = 1 - \frac{\rho c_0^2}{\lambda + 2\mu}, \quad (2.11)$$

all solutions have the form

$$U(\theta, x_2, T) = \sum_{k \in \mathbf{Z}^*} a(k, T) e^{ik\theta} \hat{v}(k, x_2), \quad (2.12)$$

where $\mathbf{Z}^* = \mathbf{Z} \setminus \{0\}$ and $\hat{v}(k, x_2) = [\hat{v}_1(k, x_2), \hat{v}_2(k, x_2)]$, with

$$\begin{aligned} \hat{v}_1(k, x_2) &= i \operatorname{sgn}(k) \left(-A e^{-|k|Ax_2} + \frac{2A}{A^2 + 1} e^{-|k|Bx_2} \right), \\ k &\in \mathbf{Z}^*, \end{aligned} \quad (2.13)$$

$$\hat{v}_2(k, x_2) = \left(e^{-|k|Ax_2} - \frac{2AB}{A^2 + 1} e^{-|k|Bx_2} \right), \quad k \in \mathbf{Z}^*. \quad (2.14)$$

To obtain real elastic displacements, we require that $a^*(k, T) = a(-k, T)$, $\forall k \in \mathbf{Z}^*$. The coefficients $a(k, T)$ are otherwise arbitrary, and can be determined by the elastic displacement at the surface ∂D . For instance, $U_1(\theta, 0, T)$ can be arbitrary, and once specified, $U_2(\theta, 0, T)$ and the displacement U in the interior of D are completely determined. For U independent of T , (2.12) describes linear traveling wave solutions (Rayleigh waves).

Matching the order ϵ^2 terms of (2.1), (2.2) with expansion (2.8) we obtain

$$\begin{aligned} \nabla \cdot \tau^L(\tilde{U}) - \rho c_0^2 \partial_\theta^2 \tilde{U} &= F(U) \quad \text{in } D, \\ \tau^L(\tilde{U}) \cdot \hat{n} &= f(U) \quad \text{at } \partial D, \end{aligned} \quad (2.15)$$

with

$$\begin{aligned} F(U) &= -\rho c_0 \partial_T \partial_\theta U - \nabla \cdot \tau^{\text{NL}}(U, U), \\ f(U) &= -\tau^{\text{NL}}(U, U) \cdot \hat{n}, \end{aligned} \quad (2.16)$$

and U a solution of the homogeneous system (2.9), (2.10). We require that $\tilde{U}(\theta, x_2) \rightarrow 0$ as $x_2 \rightarrow \infty$.

In order for (2.15), (2.16) to have a solution, $F(\theta, x_2, T) = F(U(\theta, x_2, T))$, $f(\theta, T) = f(U(\theta, 0, T))$

must satisfy the solvability condition

$$\int_D u^*(\theta, x_2, T) \cdot F(\theta, x_2, T) - \int_{\partial D} u^*(\theta, 0, T) \cdot f(\theta, T) = 0 \quad (2.17)$$

for all solutions $u(\theta, x_2, T)$ of the homogeneous system (see [3]). Equivalently, letting $v_k(x_2) = e^{ik\theta} \times \hat{v}(k, x_2)$, with the components of $\hat{v}(k, x_2)$ as in (2.13), (2.14), we require

$$\begin{aligned} & 2\rho c_0 \partial_T \int_D v_k^*(x_2) \cdot \partial_\theta U \\ &= - \int_D v_k^*(x_2) \cdot (\nabla \cdot \tau^{\text{NL}}(U, U)) \\ &+ \int_{\partial D} v_k^*(0) \cdot (\tau^{\text{NL}}(U, U) \cdot \hat{n}) \end{aligned} \quad (2.18)$$

for all $k \in \mathbf{Z}^*$.

The amplitude equation (2.18) is the desired equation for the evolution of the coefficients $a(k, T)$, $k \in \mathbf{Z}^*$, of the lowest-order displacement $U(\theta, x_2, T)$ in the “slow” time scale $T = \epsilon t$. The initial conditions $a(k, 0)$ should satisfy the reality conditions $a(-k, 0) = a^*(k, 0)$, $\forall k \in \mathbf{Z}^*$. Note that the assumption that the material is hyperelastic has not been used so far, and that (2.18) involves only the quadratic non-linearity of the equations of motion, even in the presence of higher-order terms.

3. Hamiltonian structure of the amplitude equation

In this section we point out some general features of the amplitude equation (2.15) that do not depend on the detailed form of the stress tensor. First, we note that in the case where the material is hyperelastic, amplitude equation (2.18) has a Hamiltonian structure.

Proposition 3.1. *Let $U(\theta, T)$ be an arbitrary solution of the linear homogeneous system (2.9), (2.10), i.e., a real function of form (2.12). Then amplitude equation (2.18) can be written as Hamilton’s equation*

$$\frac{da(k)}{dT} = -i \operatorname{sgn}(k) \frac{\partial H}{\partial a(-k)}, \quad k \in \mathbf{Z}^*. \quad (3.1)$$

The Hamiltonian H is given by

$$H = (K)^{-1} \int_D W^{\text{NL}}(U, U, U), \quad (3.2)$$

with $K = 4\rho c_0 \pi d$, and d a constant ($d = |k| \times \int_0^\infty (|\hat{v}_1(k, x_2)|^2 + |\hat{v}_2(k, x_2)|^2)$).

Proof. Let $V(a(k)) = \int_D W^{\text{NL}}(U, U, U)$ be the cubic potential energy, restricted to the space of solutions U of the linear homogeneous system (2.9), (2.10). It is easy to show (see [3]) that the right-hand side of (2.18) is the (formal) gradient of V , that is,

$$\begin{aligned} \frac{\partial V}{\partial a(-k)} &= - \int_D v(-k, x_2) \cdot (\nabla \cdot \tau^{\text{NL}}(U, U)) \\ &+ \int_{\partial D} v(-k, 0) \cdot (\tau^{\text{NL}}(U, U) \cdot \hat{n}), \end{aligned} \quad (3.3)$$

$k \in \mathbf{Z}^*$. On the other hand,

$$2\rho c_0 \partial_T \int_D \hat{v}^*(k, x_2) \cdot \partial_\theta U = 4\rho c_0 \pi d \frac{ik}{|k|} \frac{\partial a(k)}{\partial T}, \quad (3.4)$$

with d as in Appendix A, and (3.1) follows. \square

Remark 3.1. Eq. (3.1) has the form of Hamilton’s equation

$$\frac{da(k)}{dT} = [a(k), H]. \quad (3.5)$$

The conjugate variables are $a(k)$, $k \in \mathbf{Z}^*$, and the Poisson bracket $[\cdot, \cdot]$ is given by

$$\begin{aligned} [f, g] &= -i \sum_{k \in \mathbf{Z}^*} \operatorname{sgn}(k) \\ &\times \left(\frac{\partial f}{\partial a(k)} \frac{\partial g}{\partial a(-k)} - \frac{\partial g}{\partial a(k)} \frac{\partial f}{\partial a(-k)} \right). \end{aligned} \quad (3.6)$$

The axioms for Poisson brackets are verified readily for (3.6).

In (3.1) we may alternatively take the canonical variables to be $a(k)$, $a^*(k)$ with $k \in \mathbf{Z}^+$ and use the reality condition $a(-k) = a^*(k)$ to write the Hamiltonian H and the Poisson bracket in terms of the $a(k)$, $a^*(k)$, $k \in \mathbf{Z}^+$. Also, letting $q(k) = (1/2)(a(k) + a^*(k))$, $p(k) = (1/2i)(a(k) - a^*(k))$, for $k \in \mathbf{Z}^+$, we

can also write Hamilton’s equations as

$$\frac{dq(k)}{dT} = \frac{1}{2} \frac{\partial H}{\partial p(k)}, \quad \frac{dp(k)}{dT} = -\frac{1}{2} \frac{\partial H}{\partial q(k)},$$

$$k \in \mathbf{Z}^+. \tag{3.7}$$

An immediate consequence of the Hamiltonian structure of (2.18) is that

$$I = \sum_{k \in \mathbf{Z} \setminus \{0\}} |k| |a(k)|^2 \tag{3.8}$$

is conserved under the evolution: by (3.6), $[a(k), I] = -ika(k)$, i.e., I is the generator of horizontal translations. On the other hand, $\int_D W^{NL}(U, U, U)$ is translation invariant, hence $[I, H] = 0$.

A Hamiltonian H obtained from the cubic potential energy densities W^{NL} of (2.7) has the general form

$$H = \sum_{k_1, k_2, k_3 \in \mathbf{Z} \setminus \{0\}} a(k_1)a(k_2)a(k_3)(ik_1)(ik_2)(ik_3) \times \delta(k_1 + k_2 + k_3) \tilde{C}_{k_1, k_2, k_3}. \tag{3.9}$$

The coefficients $\tilde{C}_{k_1, k_2, k_3}$ can be computed easily once W^{NL} is specified, and we see that they are sums of terms

$$\frac{g(k_1, k_2, k_3)}{f_1|k_1| + f_2|k_2| + f_3|k_3|},$$

where the $g(k_1, k_2, k_3)$ depend on A, B and $\text{sgn}(k_j)$, $j = 1, 2, 3$, and the f_1, f_2, f_3 are constants (depending on A, B). Therefore, $\tilde{C}_{\lambda k_1, \lambda k_2, \lambda k_3} = \lambda^{-1} \tilde{C}_{k_1, k_2, k_3}$ for all $\lambda \in \mathbf{R}$ and $k_1, k_2, k_3 \in \mathbf{Z}^*$.

The amplitude equation will thus have the form

$$\frac{da(k)}{dT} = \sum_{k_1 \in \mathbf{Z} \setminus \{0, k\}} [ik_1 a(k_1)] [i(k - k_1) a(k - k_1)] \times (-ik) \Lambda(k, k_1), \quad k \in \mathbf{Z}^*, \tag{3.10}$$

where $\Lambda(k, k_1) = \tilde{C}_{-k, k_1, k - k_1} + \tilde{C}_{k_1, -k, k - k_1} + \tilde{C}_{k_1, k - k_1, -k}$. (The reality of the Hamiltonian implies that $\Lambda^*(k, k_1) = \Lambda(-k, -k_1)$, $\forall k, k_1 \in \mathbf{Z}^*$.) Translation invariance and the fact that the non-linearity of (3.10) is quadratic imply that, for any $L \in \mathbf{Z}^+$, the subspaces V_L of functions whose Fourier coefficients $a(k)$ vanish for $k \notin L\mathbf{Z}^*$ are invariant under the evolution of (3.10). Then, by the homogeneity of the coefficients $ik \Lambda(k, k_1)$ (and the fact that (3.10) is quadratic), if $\alpha(k, T)$ is a trajectory of (3.10) with initial condition $\alpha(k, 0) = f(k)$, and $\beta(Lk, T)$ a trajectory of (3.10)

with initial condition $\beta(Lk, 0) = rf(k)$ (for $L \in \mathbf{Z}^+$, $r \in \mathbf{R}$), we will have $\beta(Lk, T) = r\alpha(k, rL^2T)$.

Remark 3.2. Since $k \neq 0$, we may also multiply (3.10) by ik to obtain an evolution equation for the Fourier coefficients $ika(k)$ of $U' = \partial_\theta U(\theta, x_2, T)$. The evolution equation for U' has the form of a conservation law $\partial_T U' + \partial_\theta (F(U')) = 0$, with $F(U')$ a quadratic integral operator (see also [6]). Starting from (3.3) it is easy to see that the equation for U' is also a Hamiltonian system for hyperelastic media.

Remark 3.3. The amplitude equations for hyperelastic media can also be derived from a variational principle using a Lagrangian. The existence of the constants H, I then follows from Noether’s theorem (see [5]). Note also that in [9] the amplitude equations for hyperelastic media are derived directly starting from an averaged Hamiltonian. Proposition 3.1 shows that the more general multiple scales argument and approaches starting from an appropriate Hamiltonian or Lagrangian yield the same equation.

4. Singularity formation and power law spectra

In this section we study numerically the evolution of the amplitude equations for three model nonlinearities. In all three cases smooth initial surface elastic displacements develop singularities. The time of singularity formation and the nature of the singularities are studied by examining the Fourier spectra of the numerical solutions.

The first two models we consider have cubic potential energy densities W_{NL1}, W_{NL2} , with

$$W_{NL1} = \frac{1}{4}(\lambda + \mu)u_{1,1}u_{1,2}^2 \quad \text{and}$$

$$W_{NL2} = \frac{1}{4}(\lambda + \mu)(u_{1,1}u_{1,2}^2 + u_{2,2}u_{2,1}^2), \tag{4.1}$$

respectively. The parts W^L, W^{NL} for the third model are the quadratic and cubic parts of the St. Venant–Kirchhoff potential energy density W_{SVK} , given by

$$W_{SVK} = \frac{\lambda}{2}(\text{tr } \mathcal{E})^2 + \mu \text{tr } \mathcal{E}^2, \quad \text{where}$$

$$\mathcal{E} = \frac{1}{2}(\nabla u + (\nabla u)^T + (\nabla u)^T \nabla u). \tag{4.2}$$

The St. Venant–Kirchhoff material is a simple model for isotropic elastic solids (see [10, Ch. 4]), while the first two non-linearities are toy models chosen for their simplicity and are not consistent with isotropy. In all the numerical experiments below the Poisson ratio was set to $1/4$ (the corresponding Rayleigh speed is approximately $c_0^2 \sim 0.845\mu/\rho$).

To integrate the equations of motion numerically we work with the variables $q(k)$, $p(k)$, $k \in \mathbf{Z}^+$. To obtain Galerkin projections of the amplitude equation we consider Hamilton's equations (3.7) for modes with wavenumber $k \leq N$ and the truncated Hamiltonian H_N ,

$$H_N = \sum_{\substack{k_2+k_3 \leq N \\ k_2, k_3 > 0}} 2[q(k_2+k_3)q(k_2)q(k_3) - q(k_2+k_3)p(k_2)p(k_3) + p(k_2+k_3)q(k_2)p(k_3) + p(k_2+k_3)p(k_2)q(k_3)] \times (k_2+k_3)k_2k_3C(k_2, k_3). \quad (4.3)$$

The coefficients $C(k_2, k_3)$ for the three models above can be computed straightforwardly using (2.12) and (2.13). Also, the components of the elastic displacement at the surface are

$$U_1(\theta, 0, T) = \sum_{k=1}^{k \leq N} c_1[-2q(k, T) \sin k\theta - 2p(k, T) \cos k\theta], \quad (4.4)$$

$$U_2(\theta, 0, T) = \sum_{k=1}^{k \leq N} c_2[2q(k, T) \cos k\theta + 2p(k, T) \sin k\theta], \quad (4.5)$$

where

$$c_1 = -A + \frac{2A}{A^2 + 1}, \quad c_2 = 1 - \frac{2A}{A^2 + 1}.$$

Remark 4.1. From Hamilton's equations and (4.3), the subspace V_E of solutions with $q(k, T) = 0$, $\forall k \in \mathbf{Z}^+$, is invariant under the evolution. An analogous statement holds for Galerkin projections. By (4.4), (4.5) these subspaces correspond to solutions with $U_1(\theta, 0, T)$ even and $U_2(\theta, 0, T)$ odd.

The Galerkin equations were integrated numerically using a predictor–corrector multi-step method

from the LSODE package (Adams–Bashforth predictor, Adams–Moulton correction, see [14]). Global accuracy in the integration of the Galerkin system was assessed and verified using the conserved quantities H and I . The truncation error will be discussed at the end of the section.

In all numerical experiments with the three models considered we observed that smooth initial surface displacements develop singularities. Examples for the three models are shown in Figs. 1, 2 and 3. The singularities are more pronounced for the horizontal surface displacement, where we see the formation of “cusps”. These cusps develop at local extrema of U_1 and can be characterized as points where $|\partial_{\theta\theta} U_1|$ diverges, see, for instance, Fig. 4. Note that in the trajectory of Fig. 4 the local maximum of U_1 is always at $\theta = 0$, in general the local extrema were observed to move slightly from their initial conditions. The above observations suggest that there is a finite singularity time T_s when the solutions cease to be smooth.

Remark 4.2. After the cusps become visually evident, we see small scale oscillations that begin to grow to appreciable magnitudes, eventually distorting the shape of the wave. The discussion at the end the section suggests that after T_s the computed surface displacement loses accuracy due to truncation error. The problem of continuing the solutions past the conjectured singularity time T_s will not be addressed here.

To determine the singularity time T_s and also to study the nature of the singularities we look at the Fourier spectra $a(k, T) = q(k, T) + ip(k, T)$, $k \in \mathbf{Z}^+$, of the numerical solutions. We observe that at some time $T = T_L$ inside the interval where we expect to find T_s the Fourier spectrum has a power law decay, while for $T < T_L$ the spectrum decays exponentially. These observations suggest that analytic initial conditions lead to solutions that remain analytic in θ for all $T \in [0, T_L)$, and that the singularities are formed at $T = T_L$, i.e., the singularity time T_s is the numerically determined T_L .

The above scenario is suggested by the log–log plots of $|a(k, T)|$ vs. k . Initially these plots are concave (possibly at large k) or have a concave envelope. Eventually they become linear, as in Figs. 5, 6 (the latter for large k), or profiles that are enveloped by lines, as in Fig. 7. The concavity of the logarithmic plots

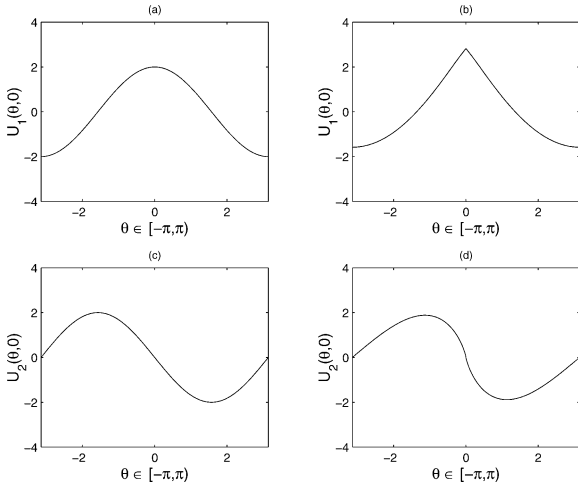


Fig. 1. Amplitude equation for model NL1: (a) Initial horizontal surface displacement $U_1(\theta, 0) = 2 \cos \theta$, (b) $U_1(\theta, T)$ at later time $T = T_1$, (c) initial vertical surface displacement $U_2(\theta, 0) = 2 \sin \theta$, (d) $U_2(\theta, T)$ at later time $T = T_1$.

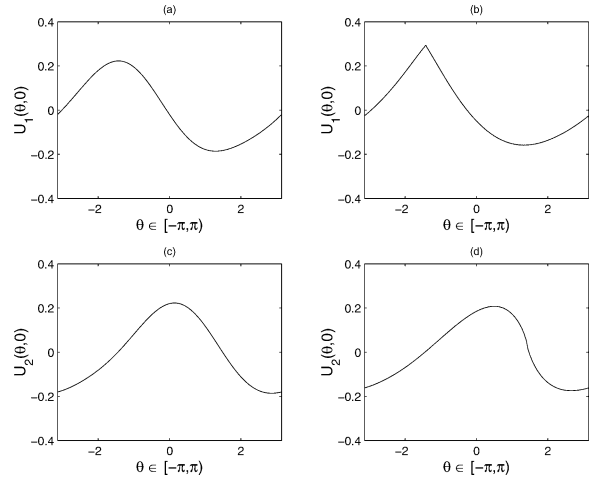


Fig. 3. Amplitude equation for St. Venant–Kirchhoff model: (a) Initial horizontal surface displacement $U_1(\theta, 0) = 0.2 \sin \theta$, (b) $U_1(\theta, T)$ at later time $T = T_1$, (c) initial vertical surface displacement $U_2(\theta, 0) = 0.2 \cos \theta$, (d) $U_2(\theta, T)$ at later time $T = T_1$.

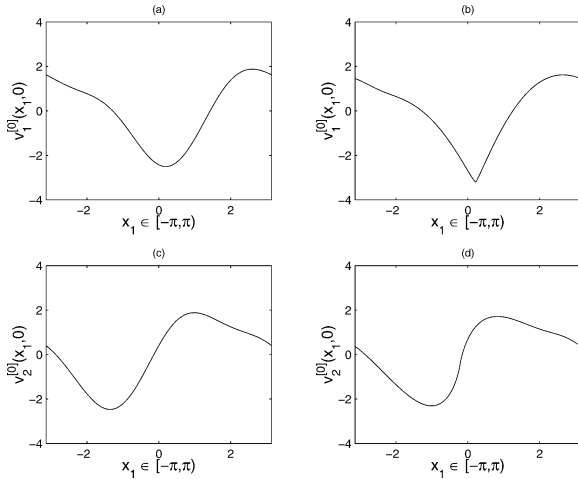


Fig. 2. Amplitude equation for model NL2: (a) Initial horizontal surface displacement $U_1(\theta, 0) = -2 \cos \theta - (1/5) \cos 2\theta - (1/5) \sin 2\theta + O(0.01)$, (b) $U_1(\theta, T)$ at later time $T = T_2$, (c) initial vertical surface displacement $U_2(\theta, 0) = 2 \sin \theta + (1/5) \cos 2\theta + (1/5) \sin 2\theta + O(0.01)$, (d) $U_2(\theta, T)$ at later time $T = T_2$.

before T_L indicates exponential decay of the power spectra for $T < T_L$. Moreover, visual inspection of the logarithmic plots already gives us T_L to a reasonable accuracy. For instance, for the NL1 model with $U(\theta, 0) \sim \cos \theta$, we can determine T_L to ± 0.05 (recall that the relevant time-scale depends on the amplitude

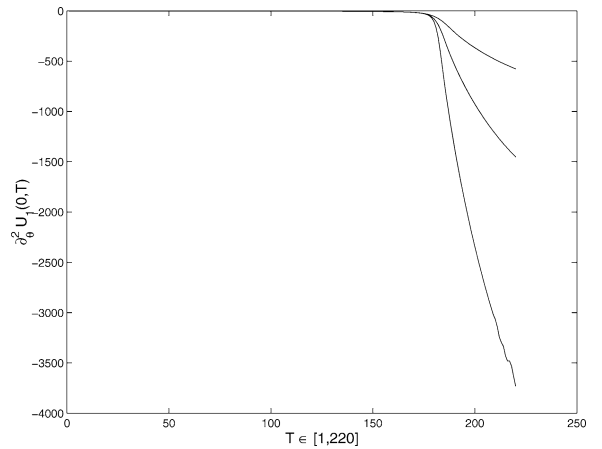


Fig. 4. Evolution of $\partial_{\theta\theta} U_1$ at $\theta = 0$ for trajectory of Fig. 1 (model NL1).

and length-scale). Note also that, to this accuracy, the times T_L obtained using different Galerkin truncations (ranging from $N = 100$ to 1600 modes) agree.

To obtain more information on the singularities we focus on trajectories that at T_L exhibit spectra $|a(k)|^2 = Ck^\gamma$ over all $k \geq 1$, e.g., as in Fig. 5. Note that such exact power law behavior at $T = T_L$ was observed for several initial conditions. Also, the spectra of such trajectories have an almost exact exponential decay before T_L , and this allows us to estimate the size of

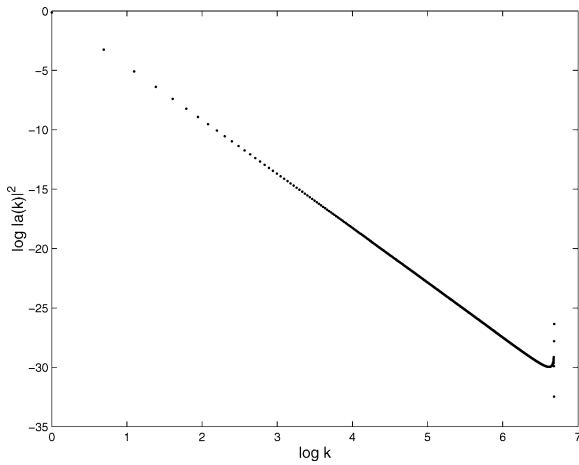


Fig. 5. Logarithmic power spectrum at $T = T_L$ for the trajectory of Fig. 1 (model NL1).

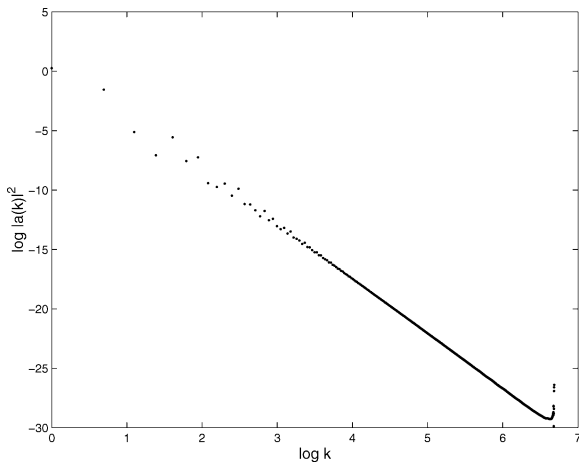


Fig. 6. Logarithmic power spectrum at $T = T_L$ for initial condition with $U_1(\theta, 0) = (11/5) \cos \theta + (3/5) \cos 2\theta - (2/5) \cos 3\theta - (1/5) \sin 3\theta + O(0.04)$ (model NL1).

the domain of analyticity of the surface elastic displacement. Recall that a periodic function $f(\theta)$ whose Fourier coefficients $\hat{f}(k)$ satisfy $|\hat{f}(k)| \leq M e^{-|k|\rho}$ for some M , $\rho > 0$ must be analytic in the strip $|\text{Im} \theta| < \rho$. We can estimate ρ by fitting the numerical values of $|a(k, T)|^2$ to a profile $C(T)k^{\gamma(T)}e^{-|k|\rho(T)}$ using least squares. The decay of $\rho(T)$ in Fig. 8 is typical. A simple way to estimate T_L is to extrapolate from the graph of $\rho(T)$. Also, we expect that as $\rho(T) \rightarrow 0$, the exponent $\gamma(T)$ converges to the power law exponent at T_L .

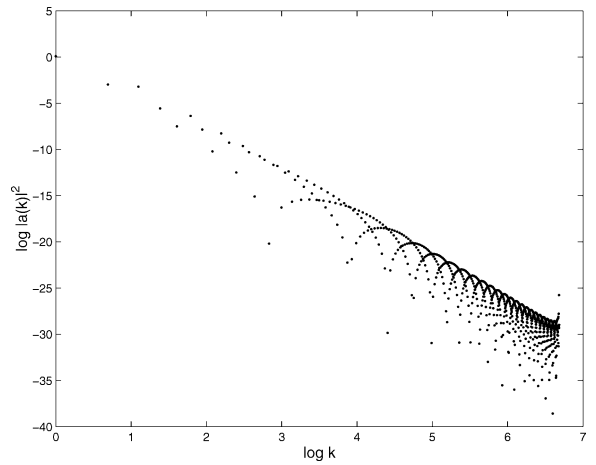


Fig. 7. Logarithmic power spectrum at $T = T_L$ from an initial condition $U_1(\theta, 0)$ with two maxima at $\theta_1, -\theta_1$. The maxima develop into cusps at the same time (model NL1).

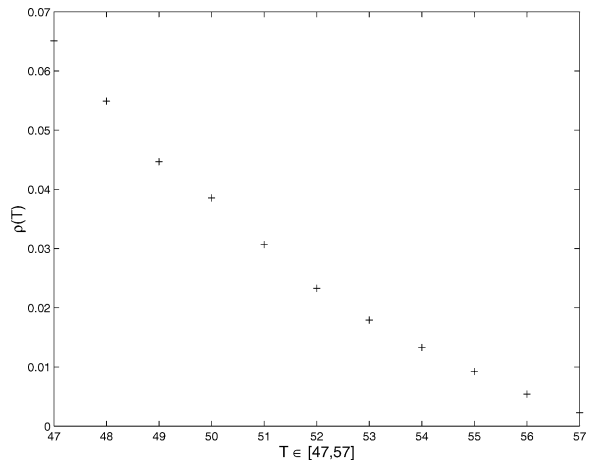


Fig. 8. Evolution of the exponent $\rho(T)$. The initial condition is $U_1(\theta, 0) = 2 \cos \theta - \sin 2\theta + O(0.05)$ (model NL1).

The time T_L and the power law exponent γ can be determined more directly, by looking for the time that minimizes the least-squares error of a linear fit to the log–log plot of the power spectrum. Assuming that the spectrum obeys an exact power law for all k , we consider only the modes with $1 \leq k \leq N/2$ to minimize the effects of the truncation error. The two approaches yield the same exponent γ , to ± 0.02 . For instance, for Fig. 5, both approaches yield $\gamma = -4.53$. Alternatively, the conservation of I and the power law

assumption imply

$$\sum_{k \in \mathbf{Z}^*} |a(1, T_L)| |k|^{1+\gamma} = I(0),$$

and we can determine γ using the numerical values of $|a(1, T_L)|, I(0)$. For the trajectory corresponding to Fig. 5, we find $\gamma = -4.52$.

The above analysis can be performed in principle for all initial conditions. For instance in Fig. 7, the envelope obeys a power law for all $k \geq 1$, and we perform the above analysis for the points on the envelope. We find the exponent $\gamma = -4.0 \pm 0.1$. However, trajectories exhibiting power law spectra at T_L only when k is sufficiently large, e.g., as in Fig. 6, require higher resolution and have not been studied systematically.

The exponents γ measured at $T = T_L$ contain interesting information on the differentiability of $U(\theta, T)$ at the singularity time $T = T_s$. Recall here that a periodic function $f(\theta)$ with Fourier coefficients $\hat{f}(k)$ satisfying $\sum_{k \in \mathbf{Z}} |\hat{f}(k)| |k|^l < \infty$ must have l continuous derivatives for all θ , i.e., must be C^l . Thus $\gamma < -4$ implies the $U(\theta, T_s)$ is C^1 . Combining this with the observed divergence of the second derivative, we thus have evidence for solutions that are analytic up to T_s , when they cease to be C^2 but remain continuously differentiable. The ‘‘cusps’’ observed in such cases are therefore somewhat misleading, the slope at the ‘‘cusp’’ points is well defined and vanishes. In the case where $\gamma = -4$, as in Fig. 7, $U(\theta, T_s)$ does not have to be C^1 , i.e., we can have bona fide cusps. The two possibilities were seen in all three models.

Remark 4.3. Note that the numerical observations are consistent with the assumptions of (2.8) used in the derivation of the amplitude equations, since U and $\partial_\theta U$ remain of $O(1)$ for all times up to T_s . In particular, we see that $\max_{\theta \in S^1} |\partial_\theta U|$ stays within 4 times its initial value. Typically, the largest increase is seen in $\partial_\theta U_2$, e.g., as in Fig. 2.

Note that in general different initial conditions lead to different power law exponents at T_s , although we have also observed initial conditions, not necessarily nearby and with well separated singularity times T_s , that lead to the same power law exponent at T_s . Further results on the dependence of the exponents on the

initial conditions and the model will be presented elsewhere.

The current simulations also give some information on traveling wave solutions $U(\theta - c_1 T, x_2)$, $c_1 \neq 0$, of the amplitude equation. Recent numerical work in [3] suggests that such solutions can exist but they are not smooth. These non-smooth traveling solutions have power law spectra with exponents $\gamma > -4$, i.e., they are more singular than the surface displacements $U(\theta, T_L)$ seen here. On the other hand, smooth initial conditions were always observed to lead to singularity formation in the present study. Smooth traveling wave solutions therefore seem to be either impossible or unstable to singularity formation. For some elastic models the amplitude equations may also have non-trivial stationary states $U(\theta)$ (see [1]). A search for trajectories that evolve (or come close) to such states has not produced any examples so far.

We conclude with a brief discussion of the reliability of the numerical results. First, the global relative numerical drifts of the conserved quantities H_N and $I_N = \sum_{k=1}^N k[q^2(k) + p^2(k)]$ over the interval of integration $[0, T_{\max}]$ (typically $T_{\max} \sim 1.2T_L$) were in the range $[10^{-8}, 10^{-7}]$, suggesting very good accuracy in the integration of the Galerkin systems. Also, as long as the number of modes N in the truncation satisfies $N > \rho(T)^{-1}$, the truncation error is insignificant (see [10]). For instance, in Fig. 8 we use $N = 800$ and the values of $\rho(T)$ in the plot are self-consistent, i.e., $\rho(T)N^{-1} \sim 1.5 \times 10^{-3}$. Determining T_s by extrapolating from these values of $\rho(T)$ should be reliable. To argue that the truncation error does not affect the lowest modes significantly as $T \rightarrow T_L$, and that the values for the time T_L and the exponent γ have sufficient accuracy, we note that the values of γ obtained using the conservation of I involved only $|a(1, T_L)|$, i.e., the least affected mode, and agree to ± 0.002 with the values of γ obtained from the modes with $1 < k < N/2$. Also, we find that the values of T_L and γ from different Galerkin truncations agree, e.g., $N = 400, 800, 1600$ give the same exponents to ± 0.002 . Finally, we integrated numerically Galerkin truncations of $u_T - (1/2)(u_\theta)^2 = 0$ with several initial conditions. We saw that T_L and the singularity time found using characteristics agree. Similar agreement between the theoretical value of T_s and T_L is also seen in the Burgers equation (see [10,11]).

5. Discussion

In the present work we have investigated some aspects of singularity formation in amplitude equations describing the slow non-linear modulation of Rayleigh waves. We observed that for analytic initial conditions solutions stay analytic up to some finite singularity time T_s , when the second derivative of the horizontal displacement diverges. The regularity of the surface elastic displacement at T_s depends in general on the initial conditions, and in some cases the wave profile is continuously differentiable at T_s . Progress on the theoretical explanation of these observations will be reported in future work.

Note that some non-local conservation laws of the type encountered here can be reduced to local equations (see, e.g., [15]). In such cases we can use characteristics to show analyticity up to the singularity time and also to trace the motion of complex singularities of the initial condition. A similar reduction to a local system does not seem applicable for surface elastic waves, however it may still be possible to trace complex singularities numerically using Padé-type extrapolations (see, e.g., [16]).

The persistence of our results for the full system is not known, and we can only say at present that the types of singularities we observed are consistent with the assumptions used in deriving the amplitude equations. It would be therefore useful to see whether we can construct exact solutions with singularities. The question could also be investigated for simpler conservation laws in the half-plane.

We conclude with some remarks on recent experimental observations of singular surface elastic waves (see [7,8]). The experiments describe pulses of surface elastic waves that develop very large slopes in $\partial_{x_1} u(x_1, 0)$. This is analogous to the blow-up of $|\partial_{\theta\theta} U|$, and we also see that the shapes of the observed pulses are qualitatively similar to the wave profiles shown in the figures, e.g., the derivative $\partial_{\theta} U$ from U in Fig. 2 is very similar to $\partial_{\theta} U$ from Figs. 1, 2

of [8]. The authors also argue that the motions they study can be approximately described by solutions of form (2.8), and show that the evolution of the pulses can be modeled quantitatively to good accuracy by a non-local conservation law for $\partial_{\theta} U$ of the type considered here, with a phenomenological dissipative term added. Thus the experiments show that the amplitude equations are a physically relevant first approximation. There are several questions however, and it appears that a more realistic model must include dissipative effects. Such effects are in evidence in the results of both studies, and should also affect the spectra (see [11]).

Acknowledgement

The author is supported by NSF grant DMS-9810751.

References

- [1] D.F. Parker, F.M. Talbot, *J. Elast.* 15 (1985) 389.
- [2] R.W. Lardner, *Int. J. Eng. Sci.* 21 (1983) 1331.
- [3] P. Panayotaros, Preprint, to appear in *Wave Motion*.
- [4] D.F. Parker, *Phys. Earth Planet. Interiors* 50 (1988) 16.
- [5] A.P. Mayer, *Phys. Rep.* 256 (1995) 237.
- [6] J.K. Hunter, *Contemp. Math.* 100 (1989) 185.
- [7] A.A. Kolomenskii, A.M. Lomonosov, R. Kuschnereit, P. Hess, V.E. Gusev, *Phys. Rev. Lett.* 79 (1997) 1325.
- [8] A.A. Kolomenskii, H.A. Schuessler, *Phys. Lett. A* 280 (2001) 157.
- [9] M.F. Hamilton, Y.A. Il'inskii, E.A. Zabolotskaya, *J. Acoust. Soc. Am.* 93 (6) (1993) 3089.
- [10] C. Sulem, P. Sulem, H. Frisch, *J. Comp. Phys.* 50 (1983) 138.
- [11] J.D. Fournier, U. Frisch, *J. Méc. Téor. Appl.* 5 (1983) 699.
- [12] P. Chadwick, *J. Elast.* 6 (1) (1976) 73.
- [13] P.G. Ciarlet, *Mathematical Elasticity, Vol. I, Three Dimensional Elasticity*, North-Holland, Amsterdam, 1988.
- [14] A.C. Hindmarsh, in: S.S. Stepleman et al. (Eds.), *Scientific Computing*, North-Holland, Amsterdam, 1983, pp. 55–64.
- [15] E.A. Kuznetsov, M.D. Spector, V.E. Zakharov, *Phys. Rev. E* 49 (1994) 1283.
- [16] R. de la Llave, S. Tombaidis, *Physica D* 71 (1994) 55.